Computer Communications 155 (2020) 184–196

Contents lists available at ScienceDirect

Computer Communications

journal homepage: www.elsevier.com/locate/comcom

UAV-enabled data acquisition scheme with directional wireless energy transfer for Internet of Things

Yalin Liu [a], Hong-Ning Dai [a,*], Hao Wang [b], Muhammad Imran [c], Xiaofen Wang [d], Muhammad Shoaib [c]

[a] Macau University of Science and Technology, Macao Special Administrative Region of China
[b] Norwegian University of Science and Technology, Gjøvik, Norway
[c] College of Applied Computer Science, King Saud University, Riyadh, Saudi Arabia
[d] Center for Cyber Security, University of Electronic Science and Technology of China, Chengdu 611731, China

ARTICLE INFO

Keywords:
Unmanned Aerial Vehicle (UAV)
Internet of Things (IoT)
Wireless Energy Transfer (WET)
Data acquisition

ABSTRACT

Low power Internet of Things (IoT) is suffering from two limitations: battery-power limitation of IoT nodes and inflexibility of infrastructure-node deployment. In this paper, we propose an Unmanned Aerial Vehicle (UAV)-enabled data acquisition scheme with directional wireless energy transfer (WET) to overcome the limitations of low power IoT. The main idea of the proposed scheme is to employ a UAV to serve as both a data collector and an energy supplier. The UAV first transfers directional wireless energy to an IoT node which then sends back the data packets to the UAV by using the harvested energy. Meanwhile, we minimize the overall energy consumption under conditions of balanced energy supply and limited overall time. Moreover, we derive the optimal values of WET time and data transmission power. After analysing the feasibility of the optimal WET time and data transmission, we design an allocation scheme based on the feasible ranges of data size level and channel-fading degree. The numerical results show the feasibility and adaptability of our allocation scheme against the varied values of multiple system parameters. We further extend our scheme to the multi-node scenario by re-designing energy beamforming and adopting multi-access mechanisms. Moreover, we also analyse the mobility of UAVs in the proposed scheme.

1. Introduction

The proliferation of Internet of Things (IoT) results in the upsurge of massive data generated from a diversity of IoT devices, such as sensor nodes, RFIDs tags and smart metres. Analysis on big volume of IoT data is bringing numerous values including forecasting disastrous events, reducing factory machine downtime, enhancing product quality and improving supply chain efficiency [1,2]. Data acquisition is a crucial step during the whole procedure of IoT data analytics while it is also challenging due to the *diversity* of IoT devices and the *heterogeneity* of IoT networks [3–5].

Recently, low power wide area network (LPWAN) has been introduced as a promising solution to achieve data acquisition in various IoT applications [6,7]. Compared with conventional IoT solutions such as Low-Power Wireless Personal Area Networks (6LoWPAN), LPWAN can significantly enhance the coverage from 100 m to 10 km. However, LPWAN also has two intrinsic limitations: 1) battery-power limitation of IoT nodes and 2) inflexibility of infrastructure-node deployment. Regarding 1), an IoT node typically has a limited battery and some of IoT nodes may even have no battery (e.g., passive RFID) [2]. IoT nodes often turn off to save energy when there is no data transmission demand [8]. Regarding 2), base stations (BS) or IoT gateways are always required to be deployed in IoT networks to achieve and facilitate network connections from IoT nodes to infrastructure nodes (e.g., BS and IoT gateways). However, the deployment of IoT infrastructure nodes results in the inflexibility and the high expenditure of establishing and maintaining the IoT network. In addition, it is also not always feasible to deploy IoT infrastructure nodes in scenarios like rural pastures, mountainous areas and ruins after disasters [9].

The recent advances in Unmanned Air Vehicle (UAV) technologies have received extensive attention from both academia and industry. UAVs have a wide diversity of applications in both military and civil fields mainly owing to their high mobility and deployment flexibility [10–14]. Many studies employ UAVs as relay nodes to extend the coverage of communications networks [15,16]. In addition, the studies such as [17,18] exploit UAVs as the data collectors hovering over the area with IoT nodes to obtain the IoT data.

* Corresponding author.
E-mail addresses: yalin_liu@foxmail.com (Y. Liu), hndai@ieee.org (H.-N. Dai), hawa@ntnu.no (H. Wang), dr.m.imran@ieee.org (M. Imran), xfwang@uestc.edu.cn (X. Wang), muhshoaib@ksu.edu.sa (M. Shoaib).

https://doi.org/10.1016/j.comcom.2020.03.020
Received 23 May 2019; Received in revised form 11 March 2020; Accepted 12 March 2020
Available online 19 March 2020

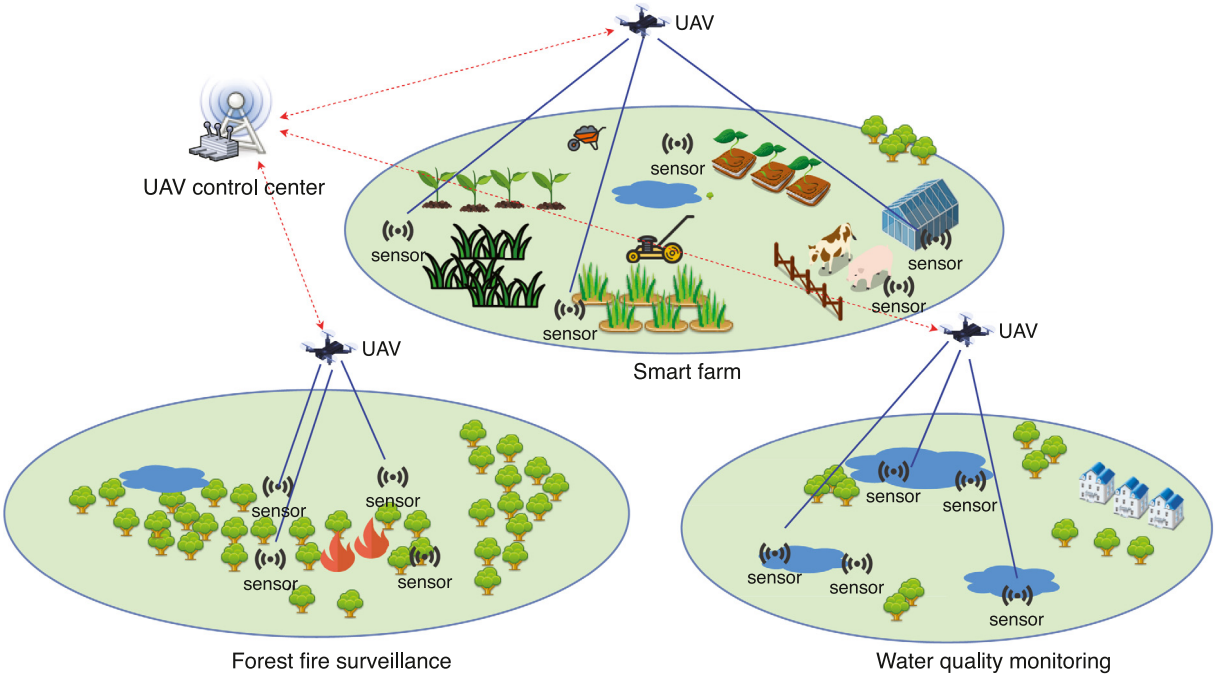

Fig. 1. Application scenarios of UAV-enabled data acquisition with WET..

On the other hand, wireless energy transfer (WET) technologies are exploited to transfer radio energy to wireless nodes so as to prolong the life-span of networks [19,20]. Since general wireless channels of WET often experience high attenuation and large path loss, recent studies tend to investigate the energy-maximization scheme to cope with different requirements. For example, recent studies [21–23] investigate maximizing the received energy at multiple users or single user. Meanwhile, [21] presents the *energy beamforming* technology that can get a maximum harvested power by controlling the transmit beamforming (BF) vector in advance.

The integration of UAV and WET technologies can overcome the aforementioned limitations of IoT data acquisition. In particular, a UAV can transfer radio energy to an IoT node which can then have enough energy to transmit data back to the UAV. During this procedure, the UAV plays a role of serving as both an energy supplier and a data collector in IoT. Accordingly, a number of IoT application scenarios can be benefited from UAV-enabled WET and data acquisition, such as forest fire surveillance, smart farms, water-quality monitoring in rural areas as shown in Fig. 1. Some recent studies exploit the integration of UAVs with WET technology (e.g., [24–27]). For example, the work of [27] investigates the optimal UAV trajectory when UAVs are used as energy suppliers to IoT nodes. However, most of existing studies assume that radio energy is broadcast omni-directionally (i.e., toward all directions) thereby leading to the poor energy harvesting efficiency.

In contrast to prior studies, this paper concentrates on designing a controllable WET by exploiting energy beamforming (BF) technology to transfer radio energy to an IoT node in a directional manner, consequently improving the energy harvesting efficiency. For the purpose of exposition, we consider the UAV-enabled data acquisition system for a single IoT node, in which the UAV transmits BF energy signal to the IoT node. The IoT node then sends back the data to the UAV by using the harvested energy. During this process, it is crucial to guarantee the optimal energy supply to complete a data acquisition task given a limited time. To this end, we aim at finding the optimal energy supply strategy to complete a data acquisition task from a UAV to an IoT node. This optimization problem is subject to sufficient energy supply and the maximum overall time. *To the best of our knowledge, this work is the first to explore the controllable WET scheme for UAV-enabled communication tasks*. The proposed scheme can be easily extended to a general scenario consisting of multiple IoT nodes and multiple UAVs, in which a UAV can transfer radio energy to IoT nodes in a merry-go-round manner (i.e., one by one) and multiple UAVs can essentially cover a wider area.

The main contributions of this paper are summarized as follows.

- *The first contribution is proposing UAV-enabled data acquisition scheme with WET*. In particular, we consider that a dispatched UAV serving as the data collector will fly over a pre-determined area containing IoT nodes and conduct data acquisition tasks. Without loss of generality, we assume that there must be a UAV control center responsible for UAV's dispatching, path planning, and the resource pre-allocation as shown in Fig. 1. When the UAV flies to an IoT node and activates the IoT node, the data acquisition task starts. We consider the UAV mounted with an antenna array with N antenna elements to generate BF energy signal for a directional WET. In order to achieve a successful and controllable task, we design a four-step communication process for every data acquisition task: 1) IoT-node activation, 2) IoT-node localization, 3) wireless energy transferring, 4) data transmission.
- *Second, we formulate an energy minimization problem to maximize the overall energy efficiency during WET and data transmission*. This optimization problem is subjected to two constraints: balanced energy supply and limited overall time. We then obtain closed-form expressions of the optimal WET time and data transmission power after solving the optimization problem. The optimal solution gives two options for adapting the different value ranges of system parameters (for simplification, we redefine a joint system parameter-channel fading degree to explain the meaning of two ranges). The first-case solution can offer a more stable energy harvesting and data transmitting power for the IoT node because it supports a more flexibly value for overall time in a better channel fading range. The second-case solution supports the fixed overall time (at its maximum value) but the data transmitting power is not so stable because of the worse channel fading range adapted in this solution.
- *Last, we design a resource allocation scheme based on the optimal solutions in the energy minimization problem*. In particular, two allocation functions are proposed to adapt the different ranges of channel fading degree. We analyse the feasibility of our scheme

by substituting the numerical values of system parameters (such as distance, path loss and fading distribution). Accordingly, we get the specific allocation values for WET time and data transmitting power. We demonstrate that our scheme is feasible since allocation parameters fall into the feasible ranges of system parameters. We also show that the allocation parameters are adjustable with the varied values of system parameters. Moreover, we also extend our analysis to the multi-node scenario and investigate the mobility of UAVs.

The rest of this paper is organized as follows. Section 2 introduces the design of the communication procedure and system models. In Section 3, we formulate the optimization problem and derive the optimal solution. Section 4 presents a feasible allocation scheme. Section 5 gives numerical results of the proposed allocation scheme and its performance. Section 6 presents the extension of our scheme for multiple nodes and discusses the mobility of UAVs. In Section 7, we conclude this paper.

2. UAV-enabled data acquisition

Section 2.1 gives communication design of a data acquisition and Section 2.2 shows the mathematical model in data acquisition.

2.1. Communication design

We assume that the trajectory path and battery storage of every UAV are pre-allocated by a remote ground control node (or a UAV control center) [28]. The UAV control center can designate UAVs to complete data acquisition tasks according to prior knowledge including the distribution of IoT nodes, locations of IoT nodes and amount of sensed data. Thus, one dispatched UAV can hover in the location of the IoT node one by one to conduct WET and data transmission along the designed path [17,18,29]. Additionally, we consider that the UAV control center pre-defines the fixed maximum threshold of energy transmit power (a.k.a. WET power for simplicity) and a maximum threshold of overall time for one task. Given the fixed WET power and a directional BF vector (mainly influenced by wireless channel), the WET time of every task depending on the energy demand of data transmission is sensitive to the wireless link. Thus, we can obtain the optimal wireless energy supply scheme by controlling WET time.

The IoT nodes may not have the data to transmit all the time (e.g., some IoT nodes may collect the data monthly), even though general communication networks in IoT can provide reliable and periodical communications. This phenomenon is especially serious for those nodes constrained by battery and coverage since they have neither enough energy nor the available data receivers. Hence, we use the radio frequency (RF) wake-up mechanism from [30,31] to provide an on-demand data acquisition, in which the UAV transmits a wake-up signal to the IoT node and then the IoT node is activated upon detecting enough power from the wake-up signal. Compared with periodic-based communications in LPWAN, RF wake-up mechanism is more flexible and suitable for data acquisition applications with sporadic transmissions especially for those IoT nodes in deployment-constrained areas.

Combining the wake-up mechanism with WET and data transmission, we design a 4-step communication process in one data acquisition task (we call it *one task* for simplicity in rest of this paper) as shown in Fig. 2. We consider that the UAV flies above an IoT node along the predefined trajectory. Then the UAV hovers over a rough position upon the IoT node and conducts a communication with the IoT node through the following four steps. In *Step 1*, the UAV wakes the IoT node up by broadcasting an activation signal [30]. In this step, the IoT node is activated by detecting enough power from the wake-up signal. In a general case, given a certain height, the received power at IoT nodes depends on the power of the wake-up signal. For simplicity, we assume that the power of the wake-up signal is large enough to activate IoT nodes. This *large enough* power value can be computed and designed by UAV control center. After *Step 1*, the IoT node then conduct *Step 2*, i.e., transmitting a feedback signal to UAV. In this step, the UAV can obtain a more specific orientation of the IoT node by analysing the feedback signal via the multi-antenna array [11,32,33]. In *Step 3*, The UAV transmits the BF energy to the IoT node. Then, in *Step 4*, the IoT node uses the harvested energy to transmit its sensed data to the UAV. Table 1 summarizes the four steps.

The first two steps are designed for activation and positioning of the IoT node, thereby paving the way for WET and data transmission. The last two steps are more crucial to accomplish data acquisition than the first two steps. It is worth noting that the wake-up time delay is much smaller than the data transmit time. As a result, the delay will not affect most opportunistic sensing applications. Recent work [31] has confirmed this observation. Additionally, to investigate a controllable energy supply, we focus on the resource allocation and modelling in last two steps. Moreover, it is necessary to fulfil two goals in last two steps: 1) *achieving the balance between the energy supply and demand*; 2) *limiting the overall time of WET and data transmission*. These two goals can be mapped to the following two conditions, respectively:

- *Balanced Energy Supply*. The harvested energy at the IoT node is required to suffice for energy consumption in data transmission. This condition can help to achieve the highest energy efficiency because the entire harvested energy is used for data transmission without waste. Note that energy supply being higher than energy consumption is a more general consideration to ensure sufficient and reliable energy supply. To simplify the analysis, we refer the (sufficient) harvested energy to the supplied energy, which is essentially equal to the consumed energy for data transmission.
- *Limited Overall Time*. The overall time spent at one data acquisition task must be smaller than the maximum threshold value to fulfil the time limitation. In this paper, the overall time is mainly composed of the WET time and the data transmission time while the time spent on the activation process is so small (e.g., 8 μs as in [34]) that it can be ignored.[1]

2.2. Communication model

Notably, in our model, we do not consider the flying/hovering power of UAVs because many recent studies such as [36–38] analysed the power consumption caused by UAVs' flying or hovering though it is much larger than that of wireless communications. Moreover, We extend the analysis to the mobile scenario of UAVs in Section 6.

2.2.1. The wireless link

We assume that a UAV is equipped with a phase-array directional antenna consisting of N antenna elements and an IoT node is equipped with a single omnidirectional antenna. Thus, the wireless link between a UAV and an IoT node can be characterized by a vector $\boldsymbol{h} \in \mathbb{C}^{N\times 1}$, where $\mathbb{C}^{N\times 1}$ denotes the space of $N \times 1$ complex matrices. We assume that the UAV hovers at a fixed position after the activation process to ensure the directional WET link to the IoT node. Besides, the communication link for ground-to-aerial (G2A) channel/aerial-to-ground (A2G) channel offers a good approximation for the practical G2A/A2G model when the UAV is above a certain altitude, which has been verified by Qualcomm [39].

[1] Kindly note that recent studies such as [31,34,35] analysed the performance (like delay and energy consumption) of the activation process of low-power IoT nodes. So, we omit the analysis of the activation process in this paper.

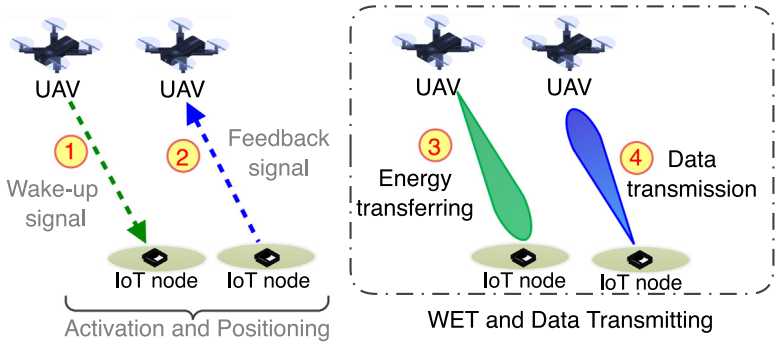

Fig. 2. A UAV-enabled data acquisition consisting of four steps.

Table 1
Four-step communication process in one task.

Step 1	The UAV broadcasts a wake-up signal to the IoT node.
Step 2	The IoT node transmits a feedback signal to the UAV.
Step 3	The UAV transmits the BF energy signal to the IoT node toward its orientation.
Step 4	The IoT node uses harvested energy to transmit its sensed data.

2.2.2. The BF energy signal

We denote the BF energy signal by $s \in \mathbb{C}^{N\times 1}$. Referring to the energy beamforming model in [21,40], the expression of BF energy signal is given by

$$s = \sqrt{P_{ET}}\mathbf{w}x,$$

where $\mathbf{w} \in \mathbb{C}^{N\times 1}$ denotes the BF vector, x denotes the normalized energy signal, and P_{ET} denotes the power spectrum density constraint for each sub-band. Referring to [40], the inequality $\|s\|_2^2 \le P_{ET}$ always holds to ensure the controllable range of WET power. In this paper, we will design $\mathbf{w}$ as a normalized vector, i.e., $\|\mathbf{w}\|_2^2 = 1$. Then P_{ET} becomes practical energy transmitting power, for simplicity, we call P_{ET} as WET power in later description.

It is worth mentioning that BF vector is used to achieve directional WET along the IoT node's orientation. BF vector can be specifically generated by using the estimated channel matrix, i.e., $\mathbf{w} = \mathbf{v}_1/\|\mathbf{v}_1\|$, where $\mathbf{v}_1$ is an eigen-vector that matches with the maximum eigenvalue λ_1 of matrix $\boldsymbol{H}$ being the co-variance matrix of $\boldsymbol{h}$, i.e., $\boldsymbol{H} = \boldsymbol{h}\boldsymbol{h}^H$. The expression $\mathbf{v}_1/\|\mathbf{v}_1\|$ comes from the energy harvesting maximum problem as given in Appendix A. The solution of this problem leads to an optimal BF vector $\mathbf{w}^*$ that contains the direction of the IoT node. The optimal BF vector leads to the maximum harvested power $\lambda_1 P_{ET}/\|\mathbf{v}_1\|^2$ at the IoT node. Hence, in rest of this paper, we use $\mathbf{v}_1/\|\mathbf{v}_1\|$ to represent the BF vector.

2.2.3. The overall time

The overall time containing WET and data transmitting is denoted by T. Let the maximum threshold of T be $T^{\max}$. Hence, $T \le T^{\max}$ represents the condition of limited overall time. Let α denote the portion part of WET time where $0 < \alpha < 1$. Then αT represents the time of WET (a.k.a. *WET time* for simplicity in the rest of this paper) and $(1-\alpha)T$ represents the time for data transmission. Note that the time of signal conversion in energy harvesting and the time in data processing can be negligible because they are much smaller than the overall time T.

2.2.4. The supplied energy

The supplied energy of one IoT node in a task is denoted by e_{EH}, which is expressed as follows,

$$e_{EH} = \zeta\alpha T\frac{\lambda_1 P_{ET}}{\|\mathbf{v}_1\|^2}, \tag{1}$$

where $0 < \zeta \le 1$ denotes the constant energy conversion efficiency that is the energy loss degree from the received signal to electric energy [22,41], αT is WET time and $\lambda_1 P_{ET}/\|\mathbf{v}_1\|^2$ is harvested power of the received signal.

2.2.5. The data transmission

We denote the data transmission power by p and denote the data transmission size by l. According to Shannon–Hartley theorem [42], we can construct the achievable data transmission rate, which is

$$r = B\log_2\left(1 + \frac{p\mathrm{tr}(\boldsymbol{H})}{N_{noise}}\right),$$

where B is the transmission bandwidth and N_{noise} is the noise power. The data transmission time is equal to l/r. We then have the time equality $l/r = (1-\alpha)T$ and further derive the expression of T as follows,

$$T = \frac{l}{(1-\alpha)r}. \tag{2}$$

We next have the consumed energy at IoT nodes during data transmission, denoted by e_{DT} as follows,

$$e_{DT} = p(1-\alpha)T. \tag{3}$$

Herein, we assume that p can be controlled by the UAV. This assumption is feasible via transmitting the expected value of p to the IoT node via the downlink.

2.2.6. Overall energy consumption

Let $e_{overall}$ be the overall energy consumption in one data acquisition task. We have

$$e_{overall} = \mathrm{tr}(\mathbf{s}\mathbf{s}^H)\alpha T = P_{ET}\mathrm{tr}(\mathbf{w}\mathbf{w}^H)\alpha T = P_{ET}\alpha T, \tag{4}$$

where $\mathbf{w}\mathbf{w}^H = \mathbf{v}_1\mathbf{v}_1^H/\|\mathbf{v}_1\|^2 = \mathbf{I}$ is the covariance matrix of $\mathbf{w}$. Obviously, the overall energy consumption in one task is equal to WET energy consumption at the UAV.

3. Problem formulation

To find out the optimal energy supply solution while maintaining high energy efficiency, we adopt the minimization of the overall energy consumption in a task as the objective and both the balanced energy supply and limited overall time as the constraints.

3.1. Energy consumption minimization problem

We mainly consider three controllable system parameters: overall time T, WET time factor α and data transmission power p. The other system parameters are either fixed as prior knowledge (such as WET power, amount of sensed data, communication bandwidth) or uncontrollable parameters (such as channel fading, noise, and energy

conversion efficiency). Here, the fixed value setting of WET power is to ensure a controllable wireless energy harvesting by only changing the WET time αT. Therefore, we construct an overall energy minimization problem by optimizing p, α and T as follows:

$$(\mathcal{P}1): \quad \min_{p,T,\alpha} \quad e_{overall} \tag{5a}$$

$$\text{s.t.} \quad e_{EH} = e_{DT}, T \in \left(0, T^{\max}\right] \tag{5b}$$

where $e_{EH} = e_{DT}$ represents a balanced energy supply for a generally consideration and $T \leq T^{\max}$ is the condition of *Limited Overall Time*. The optimal solution in $\mathcal{P}1$ can be used to adjust the data acquisition task in an optimal energy supply-and-demand. For example, multiplying the optimal data transmission power p^* by the optimal data transmission time $(1-\alpha^*)T^*$, we get the optimal energy consumption for data transmission demand; multiplying the WET power P_{ET} by the optimal WET time $\alpha^* T^*$, we get the optimal energy supply in WET.

3.2. Optimal solution

Due to fading characteristics of the wireless channel, both WET and data transmission processes are sensitive to the diverse channel fading effects, leading to unstable energy supply-and-demand in a task. Hence, we find that the optimal solution of energy supply-and-demand is related to the channel fading and also constrained by the feasible range of the channel-fading. In order to simplify the analysis of our solution, we define $\kappa \triangleq \frac{N_{noise}}{\zeta \lambda_1 P \frac{tr(\boldsymbol{H})}{\|\mathbf{v}_1\|^2}}$ as a joint channel-fading degree that will be used to represent the feasible condition of our optimal solution. Obviously, κ represents a system-fading degree in terms of the wireless channel, noise and also energy conversion. We observe that, the smaller value of κ indicates a better communication condition.

Solving $\mathcal{P}1$, we derive the optimal solution as shown in Theorem 1.

Theorem 1. *$\mathcal{P}1$ has two optimal solution for two cases:*

Case 1 If channel-fading degree κ is in the range specified as follows,

$$0 < \kappa \leq \frac{T^{\max} B}{3l} - \frac{1}{2}, \tag{6}$$

then the optimal solution is

$$T_1^{opt} = \frac{3l(2\frac{N_{noise}}{tr(\boldsymbol{H})} + \zeta \frac{\lambda_1 P_{ET}}{\|\mathbf{v}_1\|^2})}{2B\zeta \frac{\lambda_1 P_{ET}}{\|\mathbf{v}_1\|}}, \tag{7a}$$

$$p_1^{opt} = 2\frac{N_{noise}}{tr(\boldsymbol{H})}, \tag{7b}$$

$$\alpha_1^{opt} = \frac{2N_{noise}}{\zeta \frac{\lambda_1 P_{ET}}{\|\mathbf{v}_1\|^2} tr(\boldsymbol{H}) + 2N_{noise}}, \tag{7c}$$

In this case, $T_1^{opt} < T^{\max}$ always holds (i.e., the overall time is smaller than the upper limit $T^{\max}$).

Case 2 If channel-fading degree κ is in the range specified as follows

$$0 < \kappa < 2\left(1 + \frac{T^{\max} B}{l}\right), \tag{8}$$

then the optimal solution is

$$T_2^{opt} = T^{\max}, \tag{9a}$$

$$p_2^{opt} = -\frac{\zeta T^{\max} B}{l \ln(2)} \frac{\lambda_1 P_{ET}}{\|\mathbf{v}_1\|^2} W(\tau) - \frac{N_{noise}}{tr(\boldsymbol{H})}, \tag{9b}$$

$$\alpha_2^{opt} = \frac{-\frac{\zeta T^{\max} B}{l \ln(2)} \frac{\lambda_1 P_{ET}}{\|\mathbf{v}_1\|^2} W(\tau) - \frac{N_{noise}}{tr(\boldsymbol{H})}}{\zeta \frac{\lambda_1 P_{ET}}{\|\mathbf{v}_1\|^2} - \frac{\zeta T^{\max} B}{l \ln(2)} \frac{\lambda_1 P_{ET}}{\|\mathbf{v}_1\|^2} W(\tau) - \frac{N_{noise}}{tr(\boldsymbol{H})}}, \tag{9c}$$

where $W(\tau)$ is Lambert Function [43] and τ is given by

$$\tau = -\frac{N_{noise}}{tr(\boldsymbol{H})} \frac{l \ln(2)}{\zeta T^{\max} B \frac{\lambda_1 P_{ET}}{\|\mathbf{v}_1\|^2}} \times 2^{\frac{l}{T^{\max} B}\left(1 - \frac{N_{noise}}{\zeta tr(\boldsymbol{H}) \frac{\lambda_1 P_{ET}}{\|\mathbf{v}_1\|^2}}\right)}.$$

In this case, $T_2^{opt} = T^{\max}$ always holds (i.e., the overall time is equal to $T^{\max}$).

Proof. The proof for Theorem 1 is given in Appendix B. ■

Remark 1. The derivation of Theorem 1 comes from inequality of limited time condition (i.e., $T \leq T^{\max}$) and equality of energy-supply condition (i.e., $e_{EH} = e_{DT}$). In particular, there are two cases for the condition $T \leq T^{\max}$: *Case 1* for $T < T^{\max}$ and *Case 2* for $T = T^{\max}$. In addition, $e_{EH} = e_{DT}$ holds to avoid unnecessary energy consumption from UAV and also satisfy the minimized overall energy consumption. Caused by energy-supply equality $\alpha^{opt} T^{opt} \zeta \lambda_1 P_{ET} / \|\mathbf{v}_1\|^2 = (1-\alpha^{opt}) T^{opt} p^{opt}$, a general expression between the optimal WET time factor and the optimal data transmission power denoted by $\alpha^{opt} = \frac{p^{opt}}{\zeta \frac{\lambda_1 P_{ET}}{\|\mathbf{v}_1\|^2} + p^{opt}}$. This expression always holds in two cases. We observe that the optimal WET time factor is also related to the optimal data transmission power.

3.3. Feasibility analysis

Since the overall time and the WET time factor are essentially determined by $\alpha \in (0,1)$ and $T \leq T^{\max}$, their optimal values in Theorem 1 are thereby feasible. However, no limitation on data transmission power p may lead to the in-feasibility of the optimal value of p. To ensure the feasibility of p^{opt}, we set a limit on p^{opt}. We denote the upper bound of p^{opt} by $p^{\max}$. Then the optimal values of data transmission power in two cases denoted by p_1^{opt} and p_2^{opt} are limited by $p_1^{opt} \leq p^{\max}$ and $p_2^{opt} \leq p^{\max}$, respectively. Solving two above inequalities, we derive two constraints on channel fading degree corresponding to *Case 1* and *Case 2* in Theorem 1 as follows:

$$0 < \kappa \leq \frac{p^{\max}}{2\zeta \frac{\lambda_1 P_{ET}}{\|\mathbf{v}_1\|^2}} \quad (for\ Case\ 1), \tag{10}$$

$$0 < \kappa \leq \frac{1}{\zeta \frac{\lambda_1 P_{ET}}{\|\mathbf{v}_1\|^2}} \cdot \frac{p^{\max}}{2^{\frac{l}{T^{\max} B}\left(1 + \frac{p^{\max}}{\zeta \frac{\lambda_1 P_{ET}}{\|\mathbf{v}_1\|^2}}\right)} - 1} \quad (for\ Case\ 2). \tag{11}$$

Plugging Eq. (10) into the previous constraint Eq. (6), we update the feasible channel-fading range for *Case 1* as

$$0 < \kappa \leq \min\left(\frac{T^{\max} B}{3l} - \frac{1}{2}, \frac{p^{\max}}{2\zeta \frac{\lambda_1 P_{ET}}{\|\mathbf{v}_1\|^2}}\right). \tag{12}$$

Meanwhile, plugging Eq. (11) into Eq. (8), we obtain the feasible channel-fading range for *Case 2* as

$$0 < \kappa < \min\left(2 + \frac{2T^{\max} B}{l}, \frac{1}{\zeta \frac{\lambda_1 P_{ET}}{\|\mathbf{v}_1\|^2}} \times \frac{p^{\max}}{2^{\frac{l}{T^{\max} B}\left(1 + \frac{p^{\max}}{\zeta \frac{\lambda_1 P_{ET}}{\|\mathbf{v}_1\|^2}}\right)} - 1}\right). \tag{13}$$

Up to now, we have obtained two optimal solutions in Theorem 1 and two updated feasible ranges of channel-fading degree κ. We can allocate the optimal values of WET time and data transmission power as long as the practical channel-fading degree is within the feasible ranges. The only remaining problem is to conduct the statistic analysis for optimal solution and to find its feasibility for practical deployment. We will analyse this issue in the next section.

4. The allocation design

In this section, we will first conduct the statistic analysis for the optimal solution and then design our allocation scheme through the analytical results.

Table 2
Parameter settings.

Fixed parameters	Values
Maximum overall time	$T^{\max} = 1$ s
Transmitting bandwidth	$B = 15$ MHz
The carrier frequency	$fc = 900$ MHz
Energy conversion efficiency	$\eta = 0.7$
Path loss exponent of LoS	$\epsilon_{LoS} = 2$
Path loss exponent of NLoS	$\epsilon_{NLoS} = 2.5$
Environment parameters	$\chi = 4.88, \xi = 0.429$
Noise Power	$N_{noise} = 10^{-9}$ W
Minimum threshold of EH power	$P_{EH\min} = -83$ dBm
WET power	$P_{ET} = 10$ W
Maximum data transmitting power	$p^{\max} = 0.1$ W
Variable Parameters	**Ranges**
the number of antenna elements	$N \in \{8, 16\}$
The UAV Height	$H_{uav} \in \{25, 50\}$ m
Data size	$l \in \{10^4, 10^5\}$ bits

4.1. Statistic analysis

Before conducting our analysis, we need to specify the channel model and system parameters, catering for the practical scenarios. In particular, we adopt the general wireless channel model $\boldsymbol{h} = \sqrt{h_0}\tilde{\boldsymbol{h}}$, with h_0 being the large-scale fading variable and $\tilde{\boldsymbol{h}} \in \mathbb{C}^{N\times 1}$ being an N-dimensional small-scale fading variable. It is worth mentioning that the small fading component may limit the practical communication range (less than 100 m) due to the energy-harvesting constraint. In addition, due to the high altitude of the UAV, h_0 depends on the probabilistic combination of Line-of-sight (LoS) and Non-line-of-sight (NLoS) links [44,45]. We derive the expression of h_0 in the following lemma.

Lemma 1. *Given the probabilistic LoS/NLoS path loss, the large-scale fading value h_0 can be given by*

$$h_0 = \left(\frac{d_0 f_c 4\pi}{c}\right)^{-2} d^{Pr_{LOS}(\epsilon_{NLoS}-\epsilon_{LoS})-\epsilon_{NLoS}},$$

where d_0 is the unit distance 1m, f_c is the carrier frequency, c is the speed of light, d is the distance from the UAV to the IoT node and P_{LoS} is the LoS probability given by $1/(1+\chi\exp(-\chi[\theta-\xi]))$. In P_{LoS}, χ, ξ are associated with the surrounding environment, θ is the UAV elevation angle that is given by $\frac{180}{\pi}\arcsin(h_{uav}/d)$, H_{uav} is the UAV height, and ϵ_{LoS}, ϵ_{NLoS} are the path loss exponents for the LoS link and the NLoS link, respectively.

Proof. The proof is given in Appendix C. ■

Moreover, we denote the additional loss of shadowing or scattering of the channel by $\tilde{\boldsymbol{h}}$, in which each entry (or element) is an independent and identically distributed (i.i.d.) circular symmetric complex Gaussian random variable with zero mean and unit variance.

We choose the system parameters as shown in Table 2, including both the fixed and variable values. Note that our approaches can also be applied to other system settings[2]. The variable parameters (including N, H_{uav}, l in Table 2) will be used as independent variables to analyse the performance of our system.

In our analysis, we adopt the minimum elevation angle of the UAV by 30°. Thus, given a fixed height H_{uav}, the UAV can cover the IoT node with the distance d. The distance d falls in the range of $(H_{uav}, H_{uav}/\sin(30°))$, which can be calculated through the triangular relation as shown in Fig. 3. For example, when the UAV flies at the height $H_{uav} = 25$ m, the distance range d falls into (25 m~50 m). Accordingly, we perform the following statistic analysis with the results being obtained by averaging over 500 randomized channel realizations. Note that the above parameters are specifically chosen though our approaches can be also applied to other system settings.

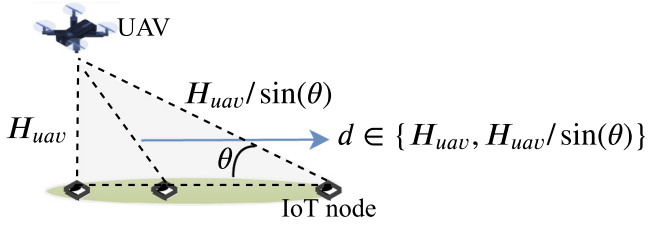

Fig. 3. Relationship between the elevation angle θ, the UAV height H_{uav} and the achievable distance d.

4.1.1. Validity of the optimal solution

We analyse the validity of feasible channel fading ranges in two cases (i.e., $(0, \kappa_1]$ and $(0, \kappa_2)$). We compare statistic results of the practical channel fading degree κ and the upper bound of two feasible ranges (i.e., κ_1 and κ_2). We then investigate whether the practical value of channel fading degree exists in two feasible ranges.

Comparing Figs. 4(a) and 4(b) (data size $l = 10^4$bits) with Figs. 4(c) and 4(d) (data size $l = 10^5$bits), respectively, we observe that the increasing value of data size leads to narrower feasible range of channel fading for both two cases of solutions. This phenomenon shows that the heavier data load brings weaker adaptability in channel fading range (because of fixed $T^{\max}B$). Meanwhile, comparing Figs. 4(a) and 4(c) (the number of antenna elements $N = 8$) with Figs. 4(b) and 4(d) (the number of antenna elements $N = 16$), respectively, we observe that the more antenna elements bring broader feasible range of channel fading for both two cases of solutions. This phenomenon indicates that we can choose a larger antenna consisting of more elements for the harsh communication environment (i.e., the worse propagation).

We also observe that there are two intersections in each sub-figure of Fig. 4. In particular, in Case 1, the upper bound of the feasible range intersects with the practical channel fading degree κ at $d = d_1$. In Case 2, the upper bound of the feasible range intersects with the practical channel fading degree κ at $d = d_2$. Accordingly, we analyse the practical range of the distance d when channel fading degree falls into two feasible ranges. First, the value of κ_1 is larger than the value of κ when $d < d_1$, implying that the first case of solution is valid and applicable under the distance limit d_1. Second, the value of κ_2 is larger than the value of κ when $d < d_1$, implying that the second case of solution is applicable under the distance limit d_2. Specifically, $d_2 = 53$ m, $d_1 = 61$ m in Fig. 4(a) while $d_2 = 68$ m, $d_1 = 72$ m in Fig. 4(b), which shows both two cases based on $l = 10^4$ bits, $N = 16$ are valid in longer distance than that when $l = 10^4$ bits, $N = 16$. Moreover, $d_1 = 34$ m in Fig. 4(c) and $d_1 = 41$ m in Fig. 4(d) show only the Case 1 is valid in their corresponding distance ranges (25 m~34 m) and (25 m~41 m). The value of d_2 is beyond the scope of Fig. 4(c) and Fig. 4(d); this means the too longer distance (longer than 25 m) resulting in Case 1.

4.1.2. Three joint parameters of the optimal solution

We observe that all optimal solutions in Theorem 1 are determined by three joint expressions, i.e., $l/T^{\max}B$, $\zeta\lambda_1 P_{ET}/\|\mathbf{v}_1\|^2$ and $N_{noise}/\mathrm{tr}(\boldsymbol{H})$. It means that a single system parameter (such as l, $T^{\max}$, B, ζ, λ_1, P_{ET}, $\|\mathbf{v}_1\|^2$, N_{noise} and $\mathrm{tr}(\boldsymbol{H})$) has no conclusive impact on optimal solution. In the same joint expression, two or more system-parameters have joint impacts on the optimal value. For instance, increasing l to 3 times and reducing $T^{\max}$ to 3 times have the same impact on the optimal solution because l and $T^{\max}B$ are in expression

[2] We choose the carrier frequency of 900 MHz to cater to longer propagation distance compared to the frequency of 2.4 GHz in the practical RF-based energy harvesting circuit [46]. In contrast, the radio signal in high carrier-frequency such as 2.4 GHz suffers the rapid propagation loss. In addition, the values of the environment parameters ($\chi = 4.88, \xi = 0.429$) are calculated through the Suburban statistic parameters $(0.1, 750, 8)$ given by [45].

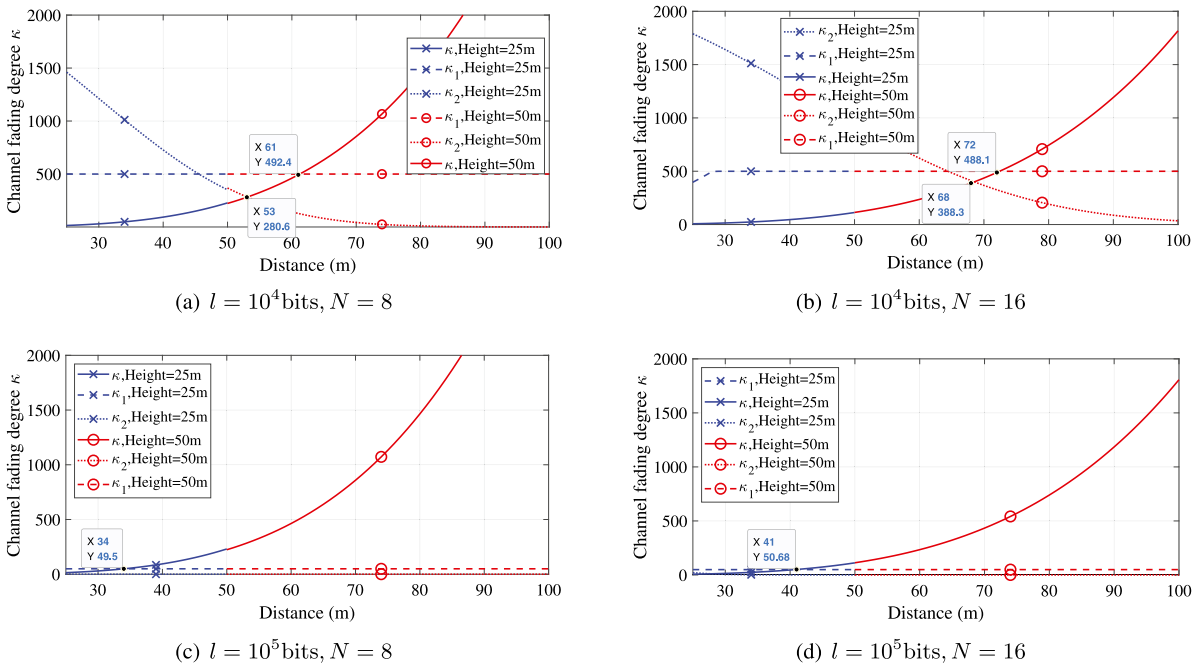

(a) $l = 10^4$bits, $N = 8$ (b) $l = 10^4$bits, $N = 16$

(c) $l = 10^5$bits, $N = 8$ (d) $l = 10^5$bits, $N = 16$

Fig. 4. Channel fading degree κ and upper bound of channel fading ranges (i.e., κ_1 and κ_2) versus the distance d, the number of antenna elements N and the data size l.

$l/T^{\max}B$. Therefore, we can analyse optimal solution based on the above three joint expressions. Meanwhile, the statistic analysis of optimal solution can also be obtained by analysing the statistic variation of those joint expressions.

For simplicity, we define three above expressions as shown in Table 3. The statistic analysis of (L_{DS}, P_{EH}, κ) is shown as follows.

- The statistic value of data size level L_{DS} is linearly influenced by $l, T^{\max}, B$. When we let $T^{\max} = 1$ and $B = 15$ MHz, the value L_{DS} will be smaller than 1 for the data size in range $0 < l <= 15$ Mbits; otherwise the value L_{DS} will be larger than 1.
- The statistic value of the harvested power P_{EH} is shown in Fig. 5(a). Obviously, the increased values of d and β lead to channel deterioration, further resulting in the decreased value of P_{EH}; the more antenna elements bring more precise orientation toward the IoT nodes, leading to the larger value of P_{EH}. In one word, the harvested power drops dramatically with the increasing distance. If the system determines the minimum threshold of harvested power $P_{EH\,\min}$, the curve of P_{EH} may intersect with a horizontal line $y = P_{EH\,\min}$ at a distance (we denote such distance as $d_{EH\,\min}$). As a result, the WET succeeds only when the distance d is shorter than the threshold $d_{EH\,\min}$. In Fig. 5(a), if $P_{EH\,\min} = -83$ dBm, the setting with $N = 16$ leads to $d_{EH\,\min} \approx 80$ m; this result implies that the WET in this situation is applicable within 80 m.
- *Statistic value of channel fading degree* κ. Fig. 5(b) shows the statistic value of κ against the distance d and the number of antenna elements N. We can see that the value of channel fading degree is increasing with the increased value of distance and the reduced number of antenna elements. Notably, comparing Fig. 5(b) with Fig. 5(a), we can see that the variation of channel fading degree is totally inverse to the received power. This phenomenon can be explained because any parameters variation causing channel deterioration can lead to the increasing value of channel fading, consequently resulting in the decreased value of the received power. Moreover, the statistic value of κ is also influenced by noise power. Moreover, the practical channel fading degree κ is restricted by the upper bound of two feasible channel fading ranges (i.e., κ_1 and κ_2). The comparison of three parameters (κ, κ_1 and κ_2) will be shown in Section 4.1.1.

Remark 2. As shown in Fig. 5(a), the supplied energy becomes very small when the transmitting distance over 100 m. This phenomenon is mainly caused by the channel propagation loss, the supplied energy decays exponentially with the increased distance [47]. Referring to [48], the power strength of RF transmission is attenuated according to the reciprocal of the distance between transmitter and receiver. For example, 20 dB per decade means with the increment of distance by 10 times, the power strength is decreased by 10^2 times. Consequently, the significant signal attenuation results in the limited power transfer distance. Moreover, the RF-to-DC energy conversion efficiency is quite low especially when the harvested RF power is small.

4.2. Allocation scheme

In Section 4.1, we derive the validity condition of the optimal solution and meanwhile obtain the statistic ranges of three joint system parameters. Accordingly, we can determine the feasible distance d and then allocate the optimal values of WET time and data transmitting power for the practical allocation.

Before presenting the allocation scheme, we first determine allocation functions of WET time an data transmitting power. After substituting three joint parameters (i.e., L_{DS}, P_{EH}, and κ) into the optimal solution of Theorem 1, two corresponding allocation functions are obtained as follows.

- *Allocation function 1*:

$$\alpha_1^{opt} T_1^{opt} = 3 L_{DS} T^{\max}, \tag{14a}$$

$$p_1^{opt} = 2\kappa P_{EH}. \tag{14b}$$

- *Allocation function 2*:

$$\alpha_2^{opt} T_1^{opt} = T^{\max} \frac{-\frac{W(\tau)}{L_{DS}\ln(2)} - \kappa}{1 - \frac{W(\tau)}{L_{DS}\ln(2)} - \kappa}, \tag{15a}$$

$$p_2^{opt} = P_{EH}\left(-\frac{W(\tau)}{L_{DS}\ln(2)} - \kappa\right), \tag{15b}$$

where

$$\tau = -\kappa L_{DS}\ln(2) \times 2^{L_{DS}(1-\kappa)}.$$

Table 3
Definition of joint system parameters.

Definition	Meaning
$L_{DS} \triangleq \frac{l}{T^{\max} B}$	The term L_{DS} represents data size level of the amount of transmitting data compared with $T^{\max} B$. Given the fixed value of maximum threshold $T^{\max}$ and bandwidth B, the larger data transmission size l leads to larger data size level L_{DS}. In this paper, we set $L_{DS} \in (0, 1)$.
$P_{EH} \triangleq \frac{\zeta \lambda_1 P_{ET}}{\|\mathbf{v}_1\|^2}$	The term P_{EH} represents the received power at IoT nodes; it depends on the energy conversion efficiency, the upper limit of WET power and the maximum orientation gain between UAV and the IoT node.
$\frac{N_{noise}}{\mathrm{tr}(\boldsymbol{H})} \triangleq \kappa P_{EH}$	This joint parameter represents the channel-fading degree of the up-link channel. For simplicity, we use the pre-defined channel-fading degree κ and P_{EH} to replace $N_{noise}/\mathrm{tr}(\boldsymbol{H})$, i.e., κP_{EH}.

Table 4
The allocation scheme for a data acquisition task.

The allocation scheme for a data acquisition task

1: Initialize system parameters $l, T^{\max}, B, P_{ET}, \eta, N_{noise}, P_{EH\min}$, and $p^{\max}$.
2: Estimate the system fading parameters $\mathrm{tr}(\boldsymbol{H}), \|\mathbf{v}_1\|^2, \lambda_1, d$.
3: Calculate the practical value of joint system parameters $L_{DS}, P_{EH}, \kappa, \kappa_1, \kappa_2$.
4: If $P_{EH} > P_{EH\min}$
5: If $\kappa \in (0, \kappa_1] \bigcap (0, \kappa_2)$
6: Using *Allocation function 1* or *Allocation function 2* to allocate WET time and data transmitting power.
7: Else if $\kappa \in (0, \kappa_1]$ and $\kappa \notin (0, \kappa_2)$
8: Using *Allocation function 1* to allocate WET time and data transmitting power.
9: End
10: End

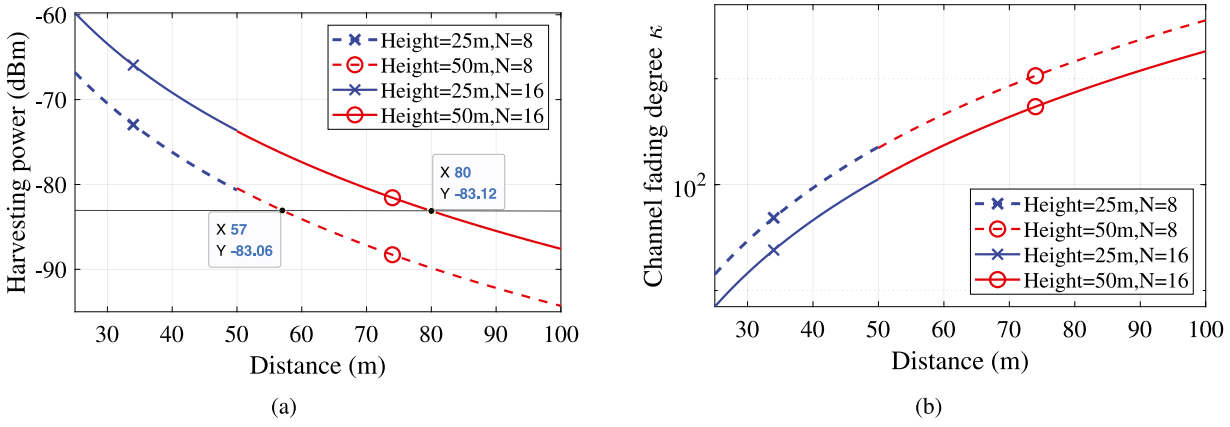

Fig. 5. Harvested power P_{EH} and channel fading degree κ versus the distance d and the number of antenna elements N.

Using the above two allocation functions, we design the allocation scheme as shown Table 4.

Remark 3. Our allocation scheme (as shown in Table 4) is based on the expressions of three joint system parameters, upper bound of channel fading degree, and also two allocation functions. By determining the feasible range of system parameters and calculating the allocation values, the proposed scheme can achieve an optimal allocation. It is worth noting that our scheme can perform well in practical scenarios because of the following three reasons.

- First, all initialized parameters are available in practical scenarios. Energy conversion efficiency η and maximum threshold of data transmitting power $p^{\max}$ are restricted by the IoT devices and hence can be regarded as the prior knowledge. Meanwhile, the noise power N_{noise} can be set as an general value, such as -160 dBm. The channel matrix $\mathrm{tr}(\boldsymbol{H})$ and the distance d can be estimated at the UAV via analysing the received feedback signal [49].
- Second, all calculated expressions $(L_{DS}, P_{EH}, \kappa, \kappa_1, \kappa_2)$ are given and verified in this paper. Therefore, the values of $L_{DS}, P_{EH}, \kappa, \kappa_1, \kappa_2$ can be calculated by substituting all specific value of basic parameters to their corresponding expressions.
- Last, the proposed scheme can offer the optimal choice after judging the feasibility of WET and the allocation function. Particularly, the condition in line 4 is used to determine whether the harvested power reaches the minimum threshold. This process is to ensure the feasibility of WET, corresponding to a restricted range $d < d_{EH\min}$ in practice. To guarantee the feasibility of two allocation functions, the condition in line 5 is to determine whether the practical channel fading degree falls into both two feasible channel fading ranges, corresponding to the restricted range $d < d_2$ in practice. Moreover, the condition in line 7 is to determine whether the practical channel fading degree is only in the feasible channel fading range of Case 2, corresponding to the restricted range $d_2 < d < d_1$ in practice.

5. Numerical results

This section presents the performance evaluation of the proposed scheme. We set the system parameters (including $T^{\max}, B, f_c, \eta, \varepsilon_{LoS}, \varepsilon_{NLoS}, \chi, \xi, N_{noise}, P_{EH\min}, P_{ET}, p^{\max}$) as the same as those in Table 2. With exceptions, we choose the fixed values for the variable parameters in Table 2 as follows: $N = 16$, $l = 10^4$ bits. For the UAV heights, we reserve two heights (25 m and 50 m) to show a constant distance range from 25 m to 100 m. Accordingly, we compute three distance

thresholds: $d_{EH\,\min} = 80$ m (i.e., valid distance bound under minimum harvested power $P_{EH\,\min}$), $d_1 = 72$ m (i.e., valid distance bound for *Allocation Function 1*) and $d_2 = 68$ m (i.e., valid distance bound for *Allocation Function 2*). Obviously, $d_2 < d_1 < d_{EH\,\min}$, implies the threshold distance of WET is larger than both two thresholds of *Allocation Function 1* and *Allocation Function 2*. Thus, according to the scheme of Table 4, we observe that *Allocation Function 1* is valid when $d <= d_1$; *Allocation Function 2* is valid when $d < d_2$. This phenomenon will be further confirmed in numerical results. In following figures, we use the solid line with a circle mark and the dashed line with a cross mark to denote numerical results under the adoption of *Allocation function 1* and *Allocation function 2*, respectively. Since all numerical figures have the same legend, so we only reserve the legend in Fig. 6(a). Furthermore, for simplicity, we use *AF 1* and *AF 2* at the legend to represent two allocation functions.

5.1. Allocation value

Fig. 6 presents comparative numerical results of two allocations against the distance d. Specifically, Fig. 6(a) and Fig. 6(b) show the allocation results of WET time and data transmitting power, respectively. We observe that all allocation values of WET time and data transmitting power under both *AF 1* and *AF 2* increase with the increased distance. This phenomenon can be explained by the fact that the IoT node requires more supplied energy to transmit its data as the increased distance leads to the deteriorated channel. In addition, we observe that *AF 1* allocates a higher data transmitting power than *AF 2*. Consequently, *AF 1* needs to allocate more WET time than *AF 2*, attributed by the relationship expression $\alpha = p/(p + P_{EH})$ in Theorem 1. As the data transmitting time is $(1-\alpha)T$, Fig. 6(c) shows a different result of data transmitting time compared with Fig. 6(a). Clearly, the data transmitting time in *AF 1* is much shorter than the data transmitting time in *AF 2*. This is because *AF 1* requires a much longer time to transmit its data than *AF 2*. It is worth noticing that the data transmitting time for both two allocations keeps nearly unchanged. This is because data transmitting power has been adaptively adjusted for the deteriorated channel, thus leading to a stable data transmission.

In summary, *AF 1* allocates more WET time and data transmitting power than *AF 2*. Thus, *AF 1* can work in a larger range than *AF 2*. Accordingly, the node allocated with *AF 1* can successfully transmit its data in less time than the node allocated with *AF 2*.

5.2. Performance analysis

Fig. 7 presents the performance of two allocation functions. We consider four performance metrics (i.e., data transmitting rate, overall latency, supplied energy, overall energy consumption) as shown in Fig. 7(b), Fig. 7(a), Figs. 7(c) and 7(d), respectively. In Fig, 7(b), we observe that, the overall latency in *AF 1* is equal to the maximum latency threshold $T^{\max} = 1s$, while the overall latency in *AF 2* is adjustable with the increased distance, which is the intrinsic setting of two allocations according to Theorem 1. In Fig. 7(a), we observe that the transmitting rate keeps stable against the distance. This is because data transmitting power has been adaptively adjusted for the deteriorated channel, thus leading to a stable data transmission. Specifically, *AF 1* that keeps a higher data transmitting rate requires more supplied energy and consumes more overall energy, compared with *AF 2*. All of these phenomenons are caused by the larger allocation values of WET time and data transmitting power of *AF 1* than *AF 2*.

Both the statistic analysis and the numerical results show multiple system parameters' impact on our scheme. Accordingly, we can improve the system performance by adjusting some parameters. For example, we can improve the harvested energy by increasing the value of WET power as well as increasing the number of antenna elements. In addition, we can improve the system adaptability to the worse channel by decreasing the size of the data load. Moreover, we can achieve the valid condition to conduct our scheme by lowering the distance between the UAV and IoT node.

6. Discussion

In this section, we extend our data acquisition scheme to the multi-node scenario and discuss the mobility of UAVs. Particularly, with the multi-node energy beamforming technology and multi-access mechanism adopted, we give an extended data acquisition task for multiple nodes. In addition, we present two mobile strategies of the UAV to deal with the nodes that are activated while cannot use the allocation scheme.

6.1. Data acquisition of multiple nodes

Recalling the aforementioned analysis in Section 4.2, we offer a data acquisition scheme to allocate WET time and data transmitting power between the UAV and one IoT node. This scheme is specifically suitable for the nodes with sparse distribution in remote area, where a UAV conducts the data acquisition tasks from multiple nodes via hovering directly above each node in one-by-one manner. Regarding another scenario that the IoT nodes are densely distributed, a UAV can fly directly above multiple nodes as close as possible to minimize path loss. In this case, the UAV may activate more than one IoT node after broadcasting the wake-up signal, then the resource allocation scheme should be adjusted to ensure the successful WET and data transmitting for multiple nodes. In particular, we consider an extended data acquisition task for multiple nodes. This task has the same activation process as the single-node task as shown in Section 2, i.e., the UAV broadcast the wake-up signal and then receive the feedback signals from multiple activated IoT nodes. In addition, we present the extension of WET and data transmitting for multiple nodes as follows: 1) the UAV transfers a BF energy signal to multiple nodes; 2) then multiple nodes with the harvested energy transmit their data to the UAV. For simplicity, we assume that the wake-up power threshold is equal to the minimum harvested power for IoT nodes. Then the activated nodes can successfully harvest the energy and then transmit their data. Fig. 8 shows the detailed arrangement of WET and data transmission of multiple nodes, in which the system parameters need to be properly assigned.

We can follow the aforementioned data acquisition scheme as Section 2 and allocate WET time and data transmitting power to ensure the successful data acquisition for each activated node. Kindly note that the previous scheme can only be used when the valid energy harvesting condition and the feasible channel fading condition are satisfied simultaneously. Meanwhile, as shown in the previous analysis in Section 4, the two conditions are essentially transformed to the distance limitations, after giving the system settings including channel fading model $\boldsymbol{h}$, energy transfer power P_{ET}, and the data transmitting size l. For the nodes that are activated at the same time, as they usually share the same channel fading model, they follow the same distance limitations (i.e., $d < \min\{d_{EH\,\min}, d_1\}$). Consequently, the n activated nodes under the distance limitations can be allocated with the corresponding WET time $\alpha_i^{alo} T_i^{alo}$ and data transmitting power p_i^{alo}, where $i \in \{1, 2, \ldots, n\}$. Moreover, the WET time should be unified as the maximal allocation value of WET time from all IoT nodes, i.e., $\max\left\{\alpha_i^{alo} T_i^{alo}\right\}$. This requirement can ensure the sufficient energy supply for all IoT nodes.

Moreover, two critical technologies should be exploited to achieve the multi-node data acquisition task: 1) energy BF for multiple nodes and 2) the multi-access mechanism for the system support for allocation of multiple nodes. Regarding energy BF technology to multiple nodes, a simple method is to combine the optimized BF vector of multiple activated nodes together and form an overall BF vector, i.e., $\mathbf{w} = \sum_{i=1}^{n} \mathbf{w}_i, \forall i \in \{1, 2, \ldots, n\}$, where $\mathbf{w}_i = \mathbf{v}_{i1} / \left\|\mathbf{v}_{i1}\right\|$ and $\mathbf{v}_{i1}$ is computed from the estimated channel matrix of each feed back signal. With respect to multi-access mechanisms, there are three types of multi-access schemes: i) frequency-division-multiple-access (FDMA) [50], ii) time-division-multiple-access (TDMA) [51], and iii) space-division-multiple-access (SDMA) [52]. It is worth mentioning that both FDMA and SDMA

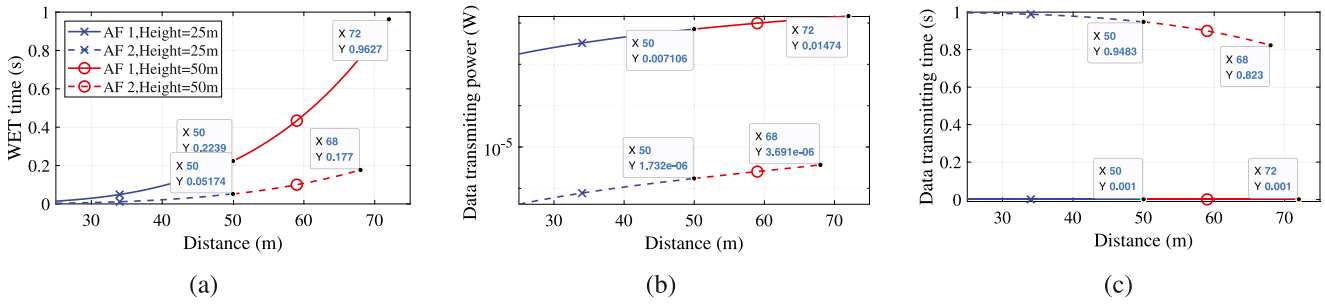

Fig. 6. WET time αT, data transmission power p and data transmitting time $(1-\alpha)T$ versus distance d.

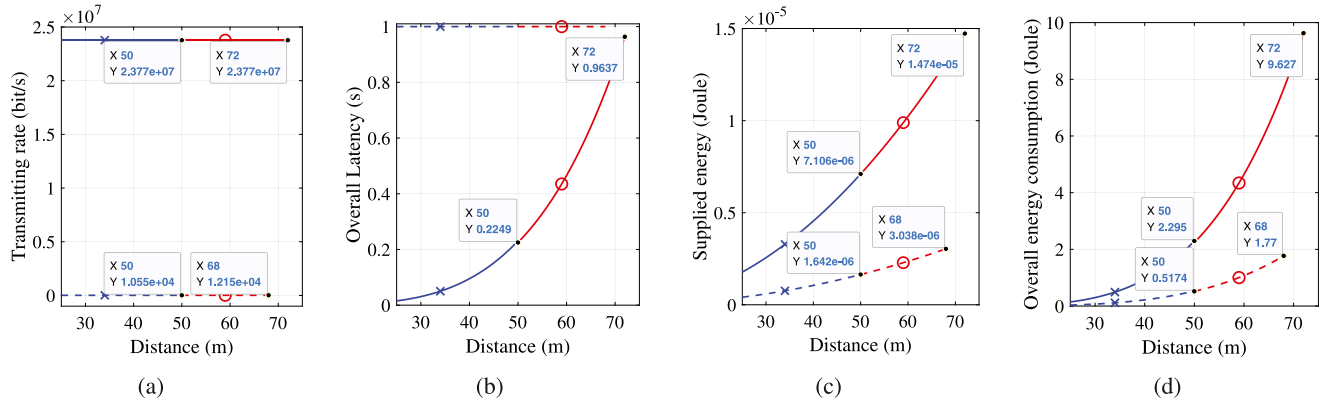

Fig. 7. Data transmitting rate r, overall latency T, supplied energy e_{EH} and overall energy consumption $e_{overall}$ versus distance d.

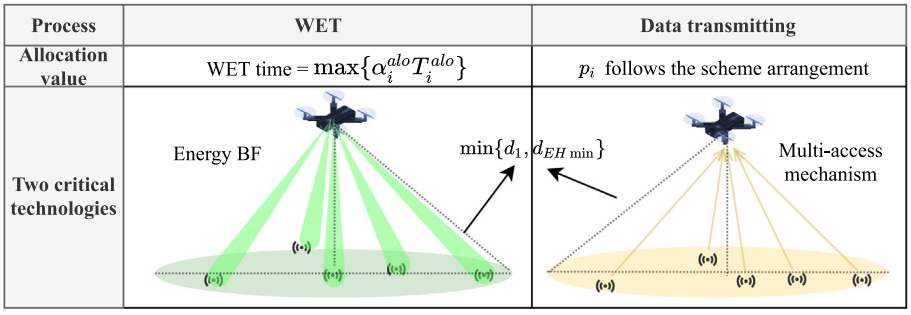

Fig. 8. Data acquisition processes of multiple nodes.

can support simultaneous G2A data transmissions, hence the allocation scheme for multiple nodes can perform independently. As a result, either FDMA or SDMA based multi-access system can independently use the allocated data transmitting power p^{alo} at each node. In contrast, TDMA requires extra time scheduling for every node. In general, we can choose the starting time of the ith node, by computing the summation of the transmission time and the starting time of the $i-1$th node, i.e., $t_i = t_{i-1} + \sum_{j=1}^{i-1}(1-\alpha_j^{alo})T_j^{alo}, \forall j = 1, 2, \ldots, i$.

6.2. Mobility analysis of UAVs

It is worth mentioning that some nodes within the distance d ($d_1 < d < d_{EH\,\min}$) cannot accomplish their data acquisition even though they are activated since these nodes do not satisfy the feasible condition that is required by the aforementioned scheme 4.2. In this case, the UAV can adjust its height or placement to shorten the distance to these nodes and then directly conduct the WET and data transmission. Considering that there may be one or more than one nodes in this scenario, we list two mobile strategies of the UAV to shorten the distance with the nodes: 1) descending height of UAV for one node; 2) trajectory planning for multiple nodes. Fig. 9 shows an analysis of the two strategies. We describe the details as follows.

Height descending strategy is adopted when the UAV directly flies above a node and its height is not low enough to satisfy the feasible condition of the data acquisition scheme. In this case, the IoT nodes are generally distributed in a sparse manner and the UAV can only activate those nodes one by one. Thus, the UAV that conduct the separate data acquisition task for each node in the one-by-one way may suffer from the case of the height being not low enough. Therefore, the UAV needs to descend its height to the distance d' ($d' < \min\{d_1, d_{EH\,\min}\}$) so as to let the allocation scheme be feasible. Additionally, trajectory planning of the UAV is used when multiple nodes are activated but only some of them satisfy the feasible distance ($d < \min\{d_1, d_{EH\,\min}\}$). This strategy can deal with the densely-distributed IoT nodes since the UAV can simultaneously activate multiple nodes while not all activated nodes fall into the feasible distance. In this case, the UAV does not need to descend its height because its height is under the feasible distance range, thus the UAV can plan its trajectory to visit the multiple nodes one by one. In particular, the trajectory planning can be determined by finding the shortest path of the UAV passing through all activated nodes. Without loss of generality, the previous studies of

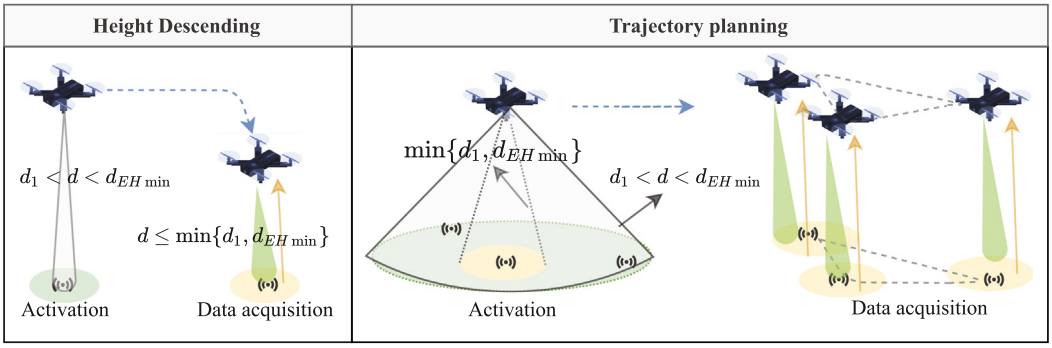

Fig. 9. Two mobility strategies of the UAV.

UAVs' trajectory planning such as [51,53] can be used to solve this issue.

7. Conclusion

This paper presents a UAV-enabled data acquisition scheme with WET for IoT. In particular, we investigate an overall energy minimization problem for a single UAV-enabled data acquisition task. We derive two allocation functions to conduct the optimal allocation of WET time and data transmission power. Accordingly, we design an allocation scheme based on the above analysis. The numerical results show that the proposed scheme can offer a flexible allocation of WET time to support the stable data transmitting power and data transmitting rate. Moreover, the proposed scheme can be extended to multiple nodes by re-designing energy BF and adopting multi-access mechanisms. Based on our allocation scheme, the feasible condition can be used to adjust the UAV's placement to collect data from all activated nodes.

Declaration of competing interest

The authors declare that they have no known competing financial interests or personal relationships that could have appeared to influence the work reported in this paper.

CRediT authorship contribution statement

Yalin Liu: Conceptualization, Formal analysis, Investigation, Methodology, Validation, Writing. **Hong-Ning Dai:** Supervision, Writing - review & editing. **Hao Wang:** Conceptualization, Investigation, Supervision, Writing. **Muhammad Imran:** Investigation, Writing - review & editing. **Xiaofen Wang:** Validation, Writing - review & editing. **Muhammad Shoaib:** Writing - review & editing.

Acknowledgments

This work was supported in part by the Macao Science and Technology Development Fund under Grant No. 0026/2018/A1, by the Deanship of Scientific Research at King Saud University through research group project number RG-1435-051, and by National Natural Science Foundation of China under Grants U1833122. The authors would like to thank G. K.-T. Hon for his constructive comments.

Appendix A

Derivation for $\mathbf{w}^*$.

The harvested power of the energy signal at the IoT node is denoted by P_{EH}. Combining WET link $\boldsymbol{h}$ with the BF energy signal $\boldsymbol{s}$, we can compute P_{EH} that is equal to $\mathrm{tr}(\boldsymbol{s}^H \boldsymbol{H}\boldsymbol{s}) = P_{ET}\mathrm{tr}(\mathbf{w}^H \boldsymbol{H}\mathbf{w})$, where $\boldsymbol{H} = \boldsymbol{h}\boldsymbol{h}^H$ is the covariance matrix of $\boldsymbol{h}$. We can compute an optimal value of $\mathbf{w}$ by maximizing the harvested power. This minimization problem can be modelled as a simple semi-definite programming problem as follows

$$\max_{\mathbf{w}} \quad P_{EH} = P_{ET}\mathrm{tr}(\mathbf{w}^H \boldsymbol{H}\mathbf{w}) \qquad \text{s.t.} \quad \mathbf{w} \succ 0.$$

The optimal solution of the above problem is $\mathbf{w}^* = \mathbf{v}_1$, where $\mathbf{v}_1$ is an eigenvector that matches with the maximum eigenvalue λ_1 of matrix H. To get a normalized BF vector for limiting the power of BF energy signal to P_{ET}, we update the optimal $\mathbf{w}^*$ as $\frac{\mathbf{v}_1}{\|\mathbf{v}_1\|}$. The updated optimal BF vector leads to the maximum harvested power $\lambda_1 P_{ET}/\|\mathbf{v}_1\|^2$ at the IoT node. ■

Appendix B

Proof of Theorem 1. The derivation steps are as follows. The objective function in $\mathcal{P}1$ (i.e., the overall energy consumption $e_{overall} = P_{ET}\alpha T$) can be reduced to WET time αT; since P_{ET} is assumed to be a fixed value as shown in the communication design of Section 2.1. Substituting the expression of T to $\mathcal{P}1$, we can reduce the three variables to two variables: α and p. Accordingly, we update $\mathcal{P}1$ to an simplified problem $\mathcal{P}2$ as follows:

$$(\mathcal{P}2): \quad \min_{p,\alpha} \quad \frac{\alpha l}{(1-\alpha)B\log_2\left(1+\frac{p\mathrm{tr}(\boldsymbol{H})}{N_{noise}}\right)}$$

$$\text{s.t.} \quad \frac{\frac{\alpha l \zeta \lambda_1 P_{ET}}{\|\mathbf{v}_1\|^2}}{(1-\alpha)B\log_2\left(1+\frac{p\mathrm{tr}(\boldsymbol{H})}{N_{noise}}\right)} = \frac{lp}{B\log_2\left(1+\frac{p\mathrm{tr}(\boldsymbol{H})}{N_{noise}}\right)},$$

$$\frac{l}{(1-\alpha)B\log_2\left(1+\frac{p\mathrm{tr}(\boldsymbol{H})}{N_{noise}}\right)} \le T^{\max}.$$

However, the objective function in above problem is non-convex to α. Therefore, we set a new variable $\beta \triangleq 1/\alpha$ to replace α. We construct a new equivalent problem $\mathcal{P}3$ as follows.

$$(\mathcal{P}3): \quad \max_{p,\beta} \quad (\beta-1)\log_2\left(1+\frac{p\mathrm{tr}(\boldsymbol{H})}{N_{noise}}\right),$$

$$\text{s.t.} \quad l\beta - (\beta-1)B\log_2\left(1+\frac{p\mathrm{tr}(\boldsymbol{H})}{N_{noise}}\right)T^{\max} \le 0,$$

$$p(\beta-1) - \frac{\zeta\lambda_1 P_{ET}}{\|\mathbf{v}_1\|^2} = 0,$$

In $\mathcal{P}3$, both objective functions and constraints are either convex or affine for all variables. Therefore, we can derive the global optimal solution of three variables (i.e., $\alpha^{opt} = 1/\beta^{opt}$, T^{opt} and p^{opt}) by Karush–Kuhn–Tucker (KKT) conditions [54].

1. Construct the Lagrange function of Problem $\mathcal{P}3$ as follows:

$$\mathcal{L}(p,\beta,\lambda,\mu) = -(\beta-1)\log_2\left(1+\frac{p\mathrm{tr}(\boldsymbol{H})}{N_{noise}}\right)$$
$$+\lambda\left(l\beta-(\beta-1)B\log_2\left(1+\frac{p\mathrm{tr}(\boldsymbol{H})}{N_{noise}}\right)T^{\max}\right)$$

$$+\ \mu\left(p(\beta-1)-\frac{\zeta\lambda_1 P_{ET}}{\|\mathbf{v}_1\|^2}\right),$$

where λ and μ are Lagrange multipliers integrating all inequality-constraints into a Lagrange function as the new objective function.

2. Compute KKT equation groups: the first-order necessary condition for two variables *(KKT 1)* and *(KKT 2)*, inequality-constraints *(KKT 3)* and Lagrange condition *(KKT 4)*, as follows

$$\partial\mathcal{L}/\partial p|_{opt}=0, \tag{KKT 1}$$

$$\partial\mathcal{L}/\partial\beta|_{opt}=0, \tag{KKT 2}$$

$$\mu^{opt}\left(p^{opt}(\beta^{opt}-1)-\zeta\frac{\lambda_1 P_{ET}}{\|\mathbf{v}_1\|^2}\right)=0,$$

$$\mu^{opt}>0,$$

$$p(\beta^{opt}-1)-\zeta\frac{\lambda_1 P_{ET}}{\|\mathbf{v}_1\|^2}=0. \tag{KKT 3}$$

$$\lambda^{opt}(l\beta^{opt}-(\beta^{opt}-1)B\log_2\left(1+\frac{p^{opt}\mathrm{tr}(\boldsymbol{H})}{N_{noise}}\right)T^{\max})=0,$$

$$\lambda^{opt}\geq 0,$$

$$l\beta^{opt}-(\beta^{opt}-1)B\log_2\left(1+\frac{p^{opt}\mathrm{tr}(\boldsymbol{H})}{N_{noise}}\right)T^{\max}\leq 0, \tag{KKT 4}$$

According to *(KKT 1)*, we have expression of μ^{opt} in $\mathcal{P}3$

$$\mu^{opt}=\frac{\lambda^{opt}T^{\max}B+1}{p+\frac{N_{noise}}{\mathrm{tr}(\boldsymbol{H})}}. \tag{16}$$

Substituting Eq. (16) to *(KKT 2)*, we obtain p^{opt} and λ^{opt} in $\mathcal{P}3$

$$\log_2\left(1+\frac{p^{opt}\mathrm{tr}(\boldsymbol{H})}{N_{noise}}\right)=\frac{\lambda^{opt}l+\frac{p^{opt}(\lambda^{opt}T^{\max}B+1)}{p^{opt}+\frac{N_{noise}}{\mathrm{tr}(\boldsymbol{H})}}}{\lambda^{opt}T^{\max}B+1} \tag{17}$$

According to Eq. (16), we determine $\mu^{opt}>0$. Then substituting $\mu^{opt}>0$ to *(KKT 3)*, we get the following equation

$$p^{opt}(\beta^{opt}-1)-\zeta\frac{\lambda_1 P_{ET}}{\|\mathbf{v}_1\|^2}=0.$$

Solving the above equation, we got the optimal value of β as follows

$$\beta^{opt}=\zeta\frac{\lambda_1 P_{ET}}{\|\mathbf{v}_1\|^2}/p^{opt}+1.$$

Since $\beta^{opt}=1/\alpha^{opt}$, we derive the optimal WET time factor of $\mathcal{P}3$ as follows

$$\alpha^{opt}=p^{opt}/(\zeta\frac{\lambda_1 P_{ET}}{\|\mathbf{v}_1\|^2}+p^{opt}). \tag{18}$$

3. For the final solution, we have two branches because of the indeterminate sign of λ^{opt}.
When $\lambda^{opt}=0$, $T^{opt}<T^{\max}$ always holds. Substituting $\lambda^{opt}=0$ to Eq. (17), we get

$$\log_2\left(1+\frac{p^{opt}\mathrm{tr}(\boldsymbol{H})}{N_{noise}}\right)=\frac{p^{opt}}{p^{opt}+\frac{N_{noise}}{\mathrm{tr}(\boldsymbol{H})}}.$$

Solving the above equation, we get the optimal data transmission power in *Case 1* of Theorem 1, i.e., $p_1^{opt}=2N_{noise}/\mathrm{tr}(\boldsymbol{H})$. Accordingly, we derive the optimal value α^{opt} by substituting p^{opt} to Eq. (18). Meanwhile, we can derive T^{opt} by substituting p^{opt} to Eq. (2) and Eq. (7a). In addition, substituting all above optimal expressions to the inequality $l\beta^{opt}-(\beta^{opt}-1)B\log_2\left(1+\frac{p^{opt}\mathrm{tr}(\boldsymbol{H})}{N_{noise}}\right)T^{\max}\leq 0$ in *(KKT 4)*, we get the feasible channel-fading range for *Case 1* of Theorem 1 in Eq. (6).
When $\lambda^{opt}>0$, $T^{opt}=T^{\max}$ always holds. Substituting $\lambda^{opt}>0$ to *(KKT4)*, we get the equation

$$l\beta-(\beta-1)B\log_2\left(1+p\mathrm{tr}(\boldsymbol{H})/N_{noise}\right)T^{\max}=0.$$

Solving the above equation, we get the optimal data transmission power as Eq. (9b) in *Case 2* of Theorem 1.
Following the similar steps of the derivation of *Case 1*, we derive the optimal value α^{opt} by substituting p^{opt} to Eq. (18). The value of T^{opt} is fixed as $T^{\max}$. Substituting all optimal expressions to Eq. (16), we get expression of λ^{opt} as

$$\lambda^{opt}=\frac{1}{\frac{l}{\log_2\left(1+\frac{p^{opt}\mathrm{tr}(\boldsymbol{H})}{N_{noise}}\right)-\frac{p^{opt}}{p^{opt}+\frac{N_{noise}}{\mathrm{tr}(\boldsymbol{H})}}}-T^{\max}B}.$$

Substituting the above equation to $\lambda^{opt}>0$, we get the feasible channel-fading range for *Case 2* of Theorem 1 in Eq. (8). ■

Appendix C

Proof of Lemma 1. The large-scale fading value h_0 can be calculated by a probability-weighted combination of path-loss components of LoS and NLoS. For convenience of calculation, we transform the dB form of the probabilistic mean path-loss model to the linear form, as follows:

$$h_0=10^{-(\frac{\mathrm{Pr}_{LOS}\mathrm{PL}_{LOS}+\mathrm{Pr}_{NLOS}\mathrm{PL}_{NLOS}}{10})}, \tag{19}$$

where Pr_{LOS} is the LoS probability, $\mathrm{Pr}_{NLOS}=1-\mathrm{Pr}_{LOS}$ is the NLoS probability, PL_{LOS} and PL_{NLOS} denote the corresponding path loss effects of LoS and NLoS links, respectively. According to the previous studies [45,55,56], PL_{LOS}, PL_{NLOS} are modelled as follows, respectively,

$$\begin{cases}\mathrm{PL}_{LOS}=\mathrm{PL}_{FS}(d_0)+10\varepsilon_{LoS}\log(d),\\ \mathrm{PL}_{NLOS}=\mathrm{PL}_{FS}(d_0)+10\varepsilon_{NLoS}\log(d),\end{cases} \tag{20}$$

where $\mathrm{PL}_{FS}(d_0)$ is the free space path loss given by $20\log(d_0 f_c 4\pi/c)$ with d_0 being the free-space reference distance, f_c being the carrier frequency and c being the speed of light. ε_{LoS} and ε_{NLoS} are the path loss exponents for LoS and NLoS links.

Substituting Eq. (20) into Eq. (19), we get the following derivation process:

$$\begin{aligned}h_0=&10^{\frac{\mathrm{Pr}_{LOS}\mathrm{PL}_{LOS}+\mathrm{Pr}_{NLOS}\mathrm{PL}_{NLOS}}{10}}\\=&10^{-\frac{\mathrm{Pr}_{LOS}10\log\left(\left(\frac{d_0 f_c 4\pi}{c}\right)^2 d^{\epsilon_{LoS}}\right)+\mathrm{Pr}_{NLOS}10\log\left(\left(\frac{d_0 f_c 4\pi}{c}\right)^2 d^{\epsilon_{NLoS}}\right)}{10}}\\=&\left(\frac{d_0 f_c 4\pi}{c}\right)^{-2\mathrm{Pr}_{LOS}} d^{-\mathrm{Pr}_{LOS}\epsilon_{LoS}}\left(\frac{d_0 f_c 4\pi}{c}\right)^{-2\mathrm{Pr}_{NLOS}} d^{-\mathrm{Pr}_{NLOS}\epsilon_{NLoS}}\\=&\left(\frac{d_0 f_c 4\pi}{c}\right)^{-2} d^{\mathrm{Pr}_{LOS}(\epsilon_{NLoS}-\epsilon_{LoS})-\epsilon_{NLoS}}.\end{aligned}$$ ■

References

[1] P.N. Borza, M. Machedon-Pisu, F. Hamza-Lup, Design of wireless sensors for IoT with energy storage and communication channel heterogeneity, Sensors 19 (15) (2019) 3364.

[2] S. Li, L. Da Xu, S. Zhao, 5G internet of things: A survey, J. Ind. Inf. Integr. 10 (2018) 1–9.

[3] L. Lan, R. Shi, B. Wang, L. Zhang, An IoT unified access platform for heterogeneity sensing devices based on edge computing, IEEE Access 7 (2019) 44199–44211.

[4] E. Ahmed, I. Yaqoob, I.A.T. Hashem, I. Khan, A.I.A. Ahmed, M. Imran, A.V. Vasilakos, The role of big data analytics in internet of things, Comput. Netw. 129 (2017) 459–471.

[5] H.-N. Dai, R.C.-W. Wong, H. Wang, Z. Zheng, A.V. Vasilakos, Big data analytics for large scale wireless networks: Challenges and opportunities, ACM Comput. Surv. (2019).

[6] K. Mekki, E. Bajic, F. Chaxel, F. Meyer, Overview of cellular LPWAN technologies for iot deployment: Sigfox, lorawan, and NB-IoT, in: 2018 IEEE International Conference on Pervasive Computing and Communications Workshops (PerCom Workshops), IEEE, 2018, pp. 197–202.

[7] Y. Mehmood, F. Ahmad, I. Yaqoob, A. Adnane, M. Imran, S. Guizani, Internet-of-things-based smart cities: Recent advances and challenges, IEEE Commun. Mag. 55 (9) (2017) 16–24.

[8] Z. Sheng, D. Tian, V.C. Leung, Toward an energy and resource efficient internet of things: A design principle combining computation, communications, and protocols, IEEE Commun. Mag. 56 (7) (2018) 89–95.
[9] K. Mekki, E. Bajic, F. Chaxel, F. Meyer, A comparative study of LPWAN technologies for large-scale IoT deployment, ICT Express 5 (1) (2019) 1–7.
[10] Y. Zeng, J. Xu, R. Zhang, Energy minimization for wireless communication with rotary-wing UAV, IEEE Trans. Wireless Commun. 18 (4) (2019) 2329–2345.
[11] W. Xu, S. Wang, S. Yan, J. He, An efficient wideband spectrum sensing algorithm for unmanned aerial vehicle communication networks, IEEE Internet Things J. 6 (2) (2018) 1768–1780.
[12] F. Shen, G. Ding, Z. Wang, Q. Wu, UAV-Based 3D spectrum sensing in spectrum-heterogeneous networks, IEEE Trans. Veh. Technol. (2019).
[13] A. Alsharoa, N.M. Neihart, S.W. Kim, A.E. Kamal, Multi-band RF energy and spectrum harvesting in cognitive radio networks, in: 2018 IEEE International Conference on Communications (ICC), IEEE, 2018, pp. 1–6.
[14] X. Liu, M. Guan, X. Zhang, H. Ding, Spectrum sensing optimization in an UAV-based cognitive radio, IEEE Access 6 (2018) 44002–44009.
[15] D. Yang, Q. Wu, Y. Zeng, R. Zhang, Energy tradeoff in ground-to-UAV communication via trajectory design, IEEE Trans. Veh. Technol. 67 (7) (2018) 6721–6726.
[16] M. Mozaffari, W. Saad, M. Bennis, M. Debbah, Mobile unmanned aerial vehicles (UAVs) for energy-efficient internet of things communications, IEEE Trans. Wireless Commun. 16 (11) (2017) 7574–7589.
[17] Q. Yang, S.J. Yoo, Optimal UAV path planning: Sensing data acquisition over iot sensor networks using multi-objective bio-inspired algorithms, IEEE Access 6 (99) (2018) 13671–13684.
[18] S. Ullah, K.-I. Kim, K.H. Kim, M. Imran, P. Khan, E. Tovar, F. Ali, UAV-Enabled healthcare architecture: Issues and challenges, Future Gener. Comput. Syst. 97 (2019) 425–432.
[19] L.R. Varshney, Transporting information and energy simultaneously, in: IEEE International Symposium on Information Theory, 2013, pp. 1612–1616.
[20] Y. Alsaba, S.K.A. Rahim, C.Y. Leow, Beamforming in wireless energy harvesting communications systems: A survey, IEEE Commun. Surv. Tutor. 20 (2) (2018) 1329–1360.
[21] R. Zhang, C.K. Ho, MIMO Broadcasting for simultaneous wireless information and power transfer, IEEE Trans. Wireless Commun. 12 (5) (2013) 1989–2001.
[22] J. Xu, R. Zhang, Energy beamforming with one-bit feedback, IEEE Trans. Signal Process. 62 (20) (2014) 5370–5381.
[23] S. Buzzi, C. D'Andrea, Energy efficiency and asymptotic performance evaluation of beamforming structures in doubly massive MIMO mmwave systems, IEEE Trans. Green Commun. Netw. 2 (2) (2018) 385–396.
[24] B. Ji, Y. Li, B. Zhou, C. Li, K. Song, H. Wen, Performance analysis of UAV relay assisted iot communication network enhanced with energy harvesting, IEEE Access 7 (2019) 38738–38747.
[25] H. Wang, J. Wang, G. Ding, L. Wang, T.A. Tsiftsis, P.K. Sharma, Resource allocation for energy harvesting-powered D2D communication underlaying UAV-assisted networks, IEEE Trans. Green Commun. Netw. 2 (1) (2018) 14–24.
[26] L. Yang, J. Chen, M.O. Hasna, H. Yang, Outage performance of UAV-assisted relaying systems with RF energy harvesting, IEEE Commun. Lett. 22 (12) (2018) 2471–2474.
[27] J. Xu, Y. Zeng, R. Zhang, UAV-Enabled wireless power transfer: Trajectory design and energy optimization, IEEE Trans. Wireless Commun. PP (99) (2017) 1–1.
[28] Y. Karaca, M. Cicek, O. Tatli, A. Sahin, S. Pasli, M.F. Beser, S. Turedi, The potential use of unmanned aircraft systems (drones) in mountain search and rescue operations, Am. J. Emerg. Med. 36 (4) (2018) 583–588.
[29] H. Hellaoui, O. Bekkouche, M. Bagaa, T. Taleb, Aerial control system for spectrum efficiency in UAV-to-cellular communications, IEEE Commun. Mag. 56 (10) (2018) 108–113.
[30] N. Kouzayha, H. Elsawy, Z. Dawy, J.G. Andrews, Analysis of an ID-based RF wake-up solution for IoT over cellular networks, in: IEEE GLOBECOM Workshops, 2017, pp. 1–6.
[31] J. Chen, Z. Dai, Z. Chen, Development of radio-frequency sensor wake-up with unmanned aerial vehicles as an aerial gateway, Sensors 19 (5) (2019) 1047.
[32] S. Rao, A. Swindlehurst, H. Pirzadeh, Massive mimo channel estimation with 1-bit spatial sigma-delta ADCS, in: ICASSP 2019-2019 IEEE International Conference on Acoustics, Speech and Signal Processing, ICASSP, IEEE, 2019, pp. 4484–4488.
[33] J. Zhao, F. Gao, L. Kuang, Q. Wu, W. Jia, Channel tracking with flight control system for UAV mmwave MIMO communications, IEEE Commun. Lett. 22 (6) (2018) 1224–1227.
[34] M. Magno, V. Jelicic, B. Srbinovski, V. Bilas, E. Popovici, L. Benini, Design, implementation, and performance evaluation of a flexible low-latency nanowatt wake-up radio receiver, IEEE Trans. Ind. Inf. 12 (2) (2016) 633–644.
[35] D. Ghose, F.Y. Li, V. Pla, MAC Protocols for wake-up radio: Principles, modeling and performance analysis, IEEE Trans. Ind. Inf. 14 (5) (2018) 2294–2306.
[36] D. Hedlund, Motor system design for large UAV, 2017, http://www.diva-portal.org/smash/get/diva2:1131267/FULLTEXT01.pdf.
[37] D.F. Finger, F. Götten, C. Braun, C. Bil, On aircraft design under the consideration of hybrid-electric propulsion systems, in: Asia-Pacific International Symposium on Aerospace Technology, Springer, 2018, pp. 1261–1272.
[38] N.S. Brun, Preliminary design of a fuel cell-battery hybrid propulsion system for a small VTOL UAV, (Master's thesis), University of Stavanger, Norway, 2018.
[39] Qualcomm, LTE Unmanned Aircraft Systems Trial Report, 2017, San Diego, CA, USA, https://www.qualcomm.com/documents/lte-unmanned-aircraft-systems-trial-report.
[40] S. Timotheou, I. Krikidis, G. Zheng, B. Ottersten, Beamforming for MISO interference channels with QoS and RF energy transfer, IEEE Trans. Wireless Commun. 13 (5) (2014) 2646–2658.
[41] F. Wang, J. Xu, X. Wang, S. Cui, Joint offloading and computing optimization in wireless powered mobile-edge computing systems, IEEE Trans. Wireless Commun. 17 (3) (2018) 1784–1797.
[42] C.E. Shannon, A mathematical theory of communication, Bell Syst. Tech. J. 27 (3) (1948) 379–423.
[43] R. Corless, G. Gonnet, D. Hare, D. Jeffrey, D. Knuth, On the lambert W function, Adv. Comput. Math. 5 (4) (1996) 329–359.
[44] A. Alsharoa, M. Yuksel, UAV-direct: Facilitating D2D communications for dynamic and infrastructure-less networking, in: Proceedings of the 4th ACM Workshop on Micro Aerial Vehicle Networks, Systems, and Applications, 2018, pp. 57–62.
[45] A. Al-Hourani, S. Kandeepan, S. Lardner, Optimal LAP altitude for maximum coverage, IEEE Wirel. Commun. Lett. 3 (6) (2014) 569–572.
[46] X. Lu, P. Wang, D. Niyato, D.I. Kim, Z. Han, Wireless networks with RF energy harvesting: A contemporary survey, IEEE Commun. Surv. Tutor. 17 (2) (2015) 757–789.
[47] S. Timotheou, G. Zheng, C. Masouros, I. Krikidis, Exploiting constructive interference for simultaneous wireless information and power transfer in multiuser downlink systems, IEEE J. Sel. Areas Commun. 34 (5) (2016) 1772–1784.
[48] X. Lu, P. Wang, D. Niyato, D.I. Kim, Z. Han, Wireless networks with RF energy harvesting: A contemporary survey, IEEE Commun. Surv. Tutor. 17 (2) (2015) 757–789.
[49] M. Biguesh, A.B. Gershman, Training-based MIMO channel estimation: a study of estimator tradeoffs and optimal training signals, IEEE Trans. Signal Process. 54 (3) (2006) 884–893.
[50] H. He, S. Zhang, Y. Zeng, R. Zhang, Joint altitude and beamwidth optimization for UAV-enabled multiuser communications, IEEE Commun. Lett. 22 (2) (2017) 344–347.
[51] C. Zhan, Y. Zeng, Completion time minimization for multi-UAV-enabled data collection, IEEE Trans. Wireless Commun. 18 (10) (2019) 4859–4872.
[52] F. Jiang, A. Swindlehurst, Optimization of UAV heading for the ground-to-air uplink, IEEE J. Sel. Areas Commun. 30 (5) (2012) 993–1005.
[53] C. Zhan, Y. Zeng, R. Zhang, Energy-efficient data collection in UAV enabled wireless sensor network, IEEE Wirel. Commun. Lett. 7 (3) (2017) 328–331.
[54] Boyd, Vandenberghe, Faybusovich, Convex optimization, IEEE Trans. Automat. Control 51 (11) (2006) 1859–1859.
[55] M. Alzenad, A. El-Keyi, H. Yanikomeroglu, 3-D placement of an unmanned aerial vehicle base station for maximum coverage of users with different QoS requirements, IEEE Wirel. Commun. Lett. 7 (1) (2017) 38–41.
[56] M. Chen, M. Mozaffari, W. Saad, C. Yin, M. Debbah, C.S. Hong, Caching in the sky: Proactive deployment of cache-enabled unmanned aerial vehicles for optimized quality-of-experience, IEEE J. Sel. Areas Commun. 35 (5) (2017) 1046–1061.